PROCEEDINGS OF SCIENCE

Quantum Error Correction and $Z(2)$ Lattice Gauge Theories

Seyong Kim *[a]

[a] *Department of Physics, Sejong University, 05006 Seoul, Republic of Korea*

E-mail: skim@sejong.ac.kr

$Z(2)$ lattice gauge theory plays an important role in the study of the threshold probability of Quantum Error Correction (QEC) for a quantum code. For certain QEC codes, such as the well-known Kitaev's toric/surface code, one can find a mapping of the QEC decoding problem onto a statistical mechanics model for a given noise model. The investigation of the threshold probability then corresponds to that of the phase diagram of the mapped statistical mechanics model. This can be studied by Monte Carlo simulation of the statistical mechanics model. In [11], we investigate the effects of realistic noise models on the toric/surface code in two dimensions together with syndrome measurement noise and introduce the random coupled-plaquette gauge model, 3-dimensional $Z(2) \times Z(2)$ lattice gauge theory. This new Z(2) gauge theory model captures main aspects of toric/surface code under depolarizing and syndrome noise. In these proceedings, we mainly focus on the aspects of Mont Carlo simulation and discuss preliminary results from Monte Carlo simulations of mapped classes of Z(2) lattice theories.

The 41st International Symposium on Lattice Field Theory (LATTICE2024)
28 July - 3 August 2024
Liverpool, UK

*In collaboration with M. Rispler (RWTH, Aachen), D. Vodola (INFN, Bologna), and M. Müller (RWTH, Aachen)

PoS(LATTICE2024)212

1. Introduction

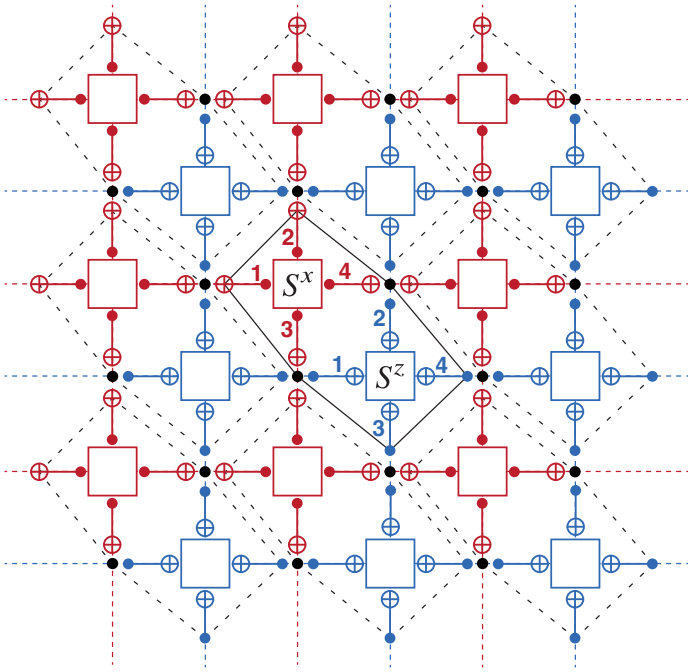

Figure 1: The layout for the data and ancilla qubits in the toric/surface code. The black dots represent the data qubits. The filled colored dot is for the control qubit of the CNOT gate and $\bigoplus$ represents the target qubit. Thus the red dots represent the ancilla qubits for the X-syndrome measurements, which acts as the control and NOT operation is performed on the data qubit. For the Z-syndrome measurements, the blue dots is the control for the CNOT gate which coincides with the data qubit and NOT operation is performed on the ancilla qubits. A syndrome measurement uses four CNOT gates. The number is the CNOT operation ordering of these four CNOT gates. Note that the results of syndrome measurements are also enumerated according to the two dimensional layout of the syndrome measurement circuit. When the syndrome information is not reliable, the syndrome bit can be flipped with a probability, q. To deal with this type of noise, syndrome measurements can be repeated adding a discrete time dimension to the model. This entails an error configuration equivalence and can be generalized to so called space-time equivalences. Here, distinct error configurations of qubit and syndrome errors are now possibly equivalent if they produce the same syndrome volume.

For certain classes of computational problems (e.g. [1, 2]), Quantum Computers (QC) are expected to outperform digital supercomputers through superposition and entanglement of quantum states due to the parallelism inherent in these quantum states. Difficult problems in lattice QCD such as real time phenomena and QCD in finite baryon density may benefit from the development of QC [2]. Constructing QC's which are competitive enough against digital supercomputers is challenging and may take decades to develop, and currently it is actively being pursued by many researchers (e.g., [3]).

To build a quantum computer, the ability to keep the qubit states stable and to change the qubit states reliably are basic requirements. Scaling up this ability to a system with a large number of qubits is also necessary [4]. Similar to bits in digital computer, qubits are susceptible to environmental effects, which leads to qubit errors. The control of qubits is a quantum mechanical evolution of the

qubit system and is also susceptible to environmental effects. In the foreseeable future, limiting these sources of errors to a negligible amount will be difficult and a fault-tolerant quantum computer architecture shall be essential in constructing quantum computers[1]. Implementing Quantum Error Correction (QEC) and error detection in quantum memory and quantum gate operation is a first step to build and operate a quantum computer in a fault-tolerant way [6, 7].

Like the Hamming code in digital computer [8], typical ideas for QEC such as the toric/surface code and topological color codes rely on forming few logical qubits out of many physical qubits. A practical question would be "how many physical qubits do we need for a logical qubit?" and notably the answer depends on the implemenation of the QEC protocol and the underlying noise model. physical qubits and physical gates which form a QEC protocol and its implementation. In this work, we investigate this problem through a mapping of this question to a statistical mechanics model where successful decoding for QEC can be identified with the existence of an 'ordered phase' and Monte Carlo (MC) simulation of the mapped model (see, e.g., [9] and [10] for some examples). A maximum allowed quantum error rate in a successful QEC protocol, called threshold probability, is related to the disorder probability of couplings (or wrong-sign couplings) and the temperature in a spin model. We specifically discuss a class of the statistical mechanics models corresponding to the decoding of quantum error patterns which may occur in the quantum circuits implementation of the toric/surface code in Fig. 1 (the toric/surface code still is one of the strong candidates for realizing fault-tolerant quantum computing among many encoding algorithms despite decades of researches on the topic). Quantum errors assumed in this work are Pauli errors (X-error or bit-flip error, Z-error or phase-flip error, Y-error or bit-flip together with phase flip error) and syndrome measurement errors (i.e., errors in the quantum circuit for the ancilla qubit measurements).

In contrast to the threshold probability obtained with leading practical decoding algorithms such as Minimum-Weight Perfect Matching (MWPM), our MC simulation results give higher threshold probability (see [11] for detail), which implies that there is a room for improvement in quantum error decoding algorithm development.

2. Method

The mapping to a statistical mechanics model proceeds with analyzing quantum error patterns in Fig. 1. In principle, Pauli errors are assumed to happen in any of data qubits and ancilla qubits and the errors in one-qubit gates and two-qubit gates (CNOT gates) can also occur. Assigning the same error probability p to qubit errors and considering how the error propagates through CNOT gates and simplifying the possibilities [11], we arrive at

$$\mathrm{pr}(X_h) = \frac{8p}{3} + \frac{48p}{15}, \qquad \mathrm{pr}(X_\mathrm{v}) = \frac{8p}{3} + \frac{32p}{15}, \qquad \mathrm{pr}(q) = \frac{8p}{3} + \frac{48p}{15} \tag{1}$$

for the case of bit-flip error, $\mathrm{pr}(X)$ (the subscript h and v denotes horizontal and vertical direction respectively), plus syndrome error $\mathrm{pr}(q)$, or for the case of phase-flip error ($\mathrm{pr}(X)$ is renamed as

[1]Note that in a modern digital computer, error detection and correction is already an essential part of the architecture (e.g., such as ECC RAM [5]) and that most digital computers do work fault-tolerantly in noisy environment when the noise level is low.

$\mathrm{pr}(Z)$) plus syndrome error, $\mathrm{pr}(q)$, and

$$\mathrm{pr}(X_h) = \frac{4p}{3} + \frac{32p}{15}, \quad \mathrm{pr}(X_\mathrm{v}) = \frac{4p}{3} + \frac{16p}{15}, \quad \mathrm{pr}(Y_h) = \frac{4p}{3} + \frac{16p}{15} = \mathrm{pr}(Y_\mathrm{v}) \tag{2}$$

$$\mathrm{pr}(Z_h) = \frac{4p}{3} + \frac{16p}{15}, \quad \mathrm{pr}(Z_\mathrm{v}) = \frac{4p}{3} + \frac{32p}{15}, \quad \mathrm{pr}(q) = \frac{8p}{3} + \frac{48p}{15} \tag{3}$$

for the case of X, Y and Z error plus syndrome error. The so-called Nishimori line (the red dotted line in Fig. 5) is the line given by

$$\exp\left(-4|J(W)|\right) = \frac{\mathrm{pr}(X)\mathrm{pr}(Y)\mathrm{pr}(Z)}{\mathrm{pr}(W)^2\mathrm{pr}(I)}, \quad \exp\left(-2|J_t{}^{\sigma,\tau}|\right) = \frac{q}{1-q}, \tag{4}$$

through the condition that the disorder distribution is equal to the thermal distribution [12].

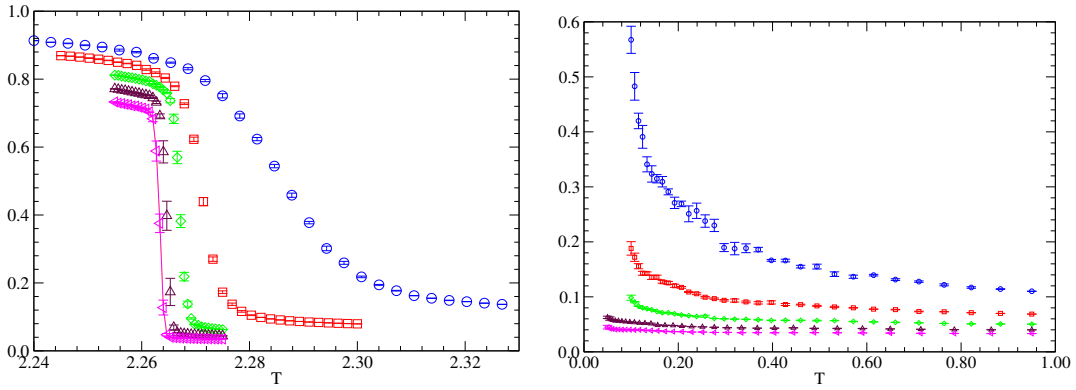

Figure 2: The Polyakov line at $p = 2.88 \times 10^{-5}$ (left) and $p = 2.31 \times 10^{-2}$ (right) for the circuit level noise. MC Simulation of $Z(2) \times Z(2)$ gauge theory on 8^3 (blue circle), 12^3 (red square), 16^3 (green diamond), 20^3 (maroon up-triangle), and 24^3 (magenta left-triangle). From Eq. 3, $\mathrm{pr}(X_h) = \frac{52p}{15} = 0.0001$ (left) and 0.08 (right).

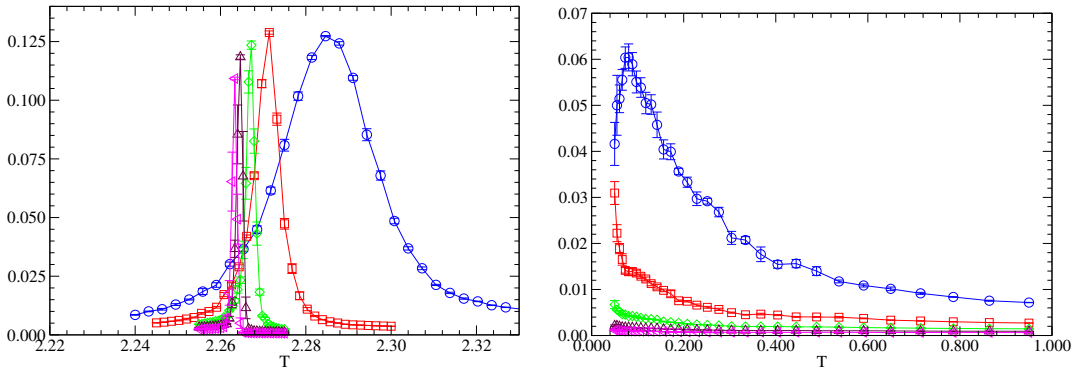

Figure 3: The Polyakov line susceptibility at $p = 2.88 \times 10^{-5}$ (left) and $p = 2.31 \times 10^{-2}$ (right). Symbols and colors are the same as in Fig. 2.

Then, the mapped statistical mechanics models can be described by the Hamiltonian

$$H = \sum_{\mathbf{n}} \left[H_X(\mathbf{n}) + H_Y(\mathbf{n}) + H_Z(\mathbf{n}) \right], \tag{5}$$

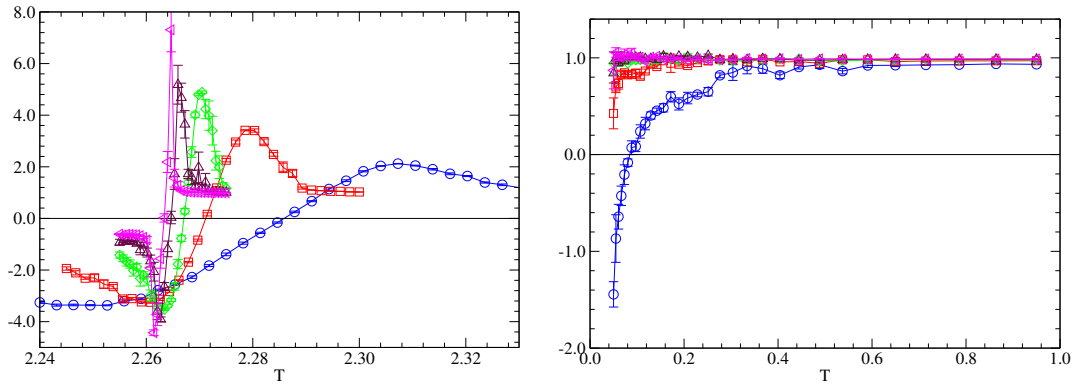

Figure 4: The third order cumulant of the Polyakov line at $p = 2.88 \times 10^{-5}$ (left) and $p = 2.31 \times 10^{-2}$ (right). Symbols and colors are the same as in Fig. 2.

where

$$\begin{aligned} H_X(\mathbf{n}) = &-J_x(\mathbf{n};X)\sigma_y(\mathbf{n})\sigma_t(\mathbf{n}+\hat{y})\sigma_y(\mathbf{n}+\hat{t})\sigma_t(\mathbf{n}) - J_y(\mathbf{n};Y)\sigma_t(\mathbf{n})\sigma_x(\mathbf{n}+\hat{t})\sigma_t(\mathbf{n}+\hat{x})\sigma_x(\mathbf{n}) \\ &-{J_t}^{\sigma}(\mathbf{n};q)\sigma_x(\mathbf{n})\sigma_y(\mathbf{n}+\hat{x})\sigma_x(\mathbf{n}+\hat{y})\sigma_y(\mathbf{n}) \\ H_Z(\mathbf{n}) = &-J_x(\mathbf{n};Z)\tau_y(\mathbf{n})\tau_t(\mathbf{n}+\hat{y})\tau_y(\mathbf{n}+\hat{t})\tau_t(\mathbf{n}) - J_y(\mathbf{n};Z)\tau_t(\mathbf{n})\tau_x(\mathbf{n}+\hat{t})\tau_t(\mathbf{n}+\hat{x})\tau_x(\mathbf{n}) \\ &-{J_t}^{\tau}(\mathbf{n};q)\tau_x(\mathbf{n})\tau_y(\mathbf{n}+\hat{x})\tau_x(\mathbf{n}+\hat{y})\tau_y(\mathbf{n}) \end{aligned} \tag{6}$$

for the X-error (bit flip) and the Z-error (phase flip) and

$$\begin{aligned} H_Y(\mathbf{n}) = &-J_x(\mathbf{n};Y)\sigma_y(\mathbf{n})\sigma_t(\mathbf{n}+\hat{y})\sigma_y(\mathbf{n}+\hat{t})\sigma_t(\mathbf{n})\tau_t(\mathbf{n}+\hat{x})\tau_x(\mathbf{n}+\hat{x}+\hat{t})\tau_t(\mathbf{n}+\hat{x}+\hat{x})\tau_x(\mathbf{n}+\hat{x}) \\ &-J_y(\mathbf{n};Y)\sigma_t(\mathbf{n})\sigma_x(\mathbf{n}+\hat{t})\sigma_t(\mathbf{n}+\hat{x})\sigma_x(\mathbf{n})\tau_y(\mathbf{n}+\hat{y})\tau_t(\mathbf{n}+\hat{y}+\hat{y})\tau_y(\mathbf{n}+\hat{y}+\hat{t})\tau_t(\mathbf{n}+\hat{y}) \end{aligned} \tag{7}$$

for the Y error (bit flip together with phase flip), where $\mathbf{n}$ denotes the location of lattice site in 3-dimension $\mathbf{n} = (i, j, k)$, and x, y denotes the spatial direction and t denotes the time direction. $\sigma_{x,y,t}(\mathbf{n})$ and $\tau_{x,y,t}(\mathbf{n})$ represent Ising spin degree of freedoms associated with the lattice site (i, j, k) for the direction of x, y, t: e.g., $\sigma_x(\mathbf{n})$ lies between the site (i, j, k) and the site $(i+1, j, k)$, and J's denote the couplings. This Hamiltonian has $Z(2) \times Z(2)$ gauge symmetry because it is invariant under $\Lambda_1\sigma\Lambda_2^{-1}$ and $\Lambda_3\tau{\Lambda_4}^{-1}$ where local $\Lambda_{1,2,3,4} \in Z(2)$. For example, to study the noise model of independent XZ plus syndrome noise, the two types of variables decouple such that we can remove the τ spin degrees of freedom from the Hamiltonian and choose $J_x(\mathbf{n};X) \neq J_y(\mathbf{n};X)$ as in Eq. 1. Then, the model becomes a 3-dimensional $Z(2)$ gauge theory with non-uniform couplings for the plaquettes, which may be called as "Random Plaquette Gauge Model (RPGM)". For the symmetric depolarizing noise case of random coupled plaquette model, we choose $J_x(\mathbf{n};X) = J_y(\mathbf{n};X) = J_x(\mathbf{n};Y) = J_y(\mathbf{n};Y) = J_x(\mathbf{n};Z) = J_y(\mathbf{n};Z) = \frac{1}{3}J_t(\mathbf{n};q)$. For the (asymmetric) depolarizing circuit-noise plus syndrome noise case of random coupled plaquette model, $J_x(\mathbf{n};X) \neq J_y(\mathbf{n};X), J_x(\mathbf{n};Z) \neq J_y(\mathbf{n};Z)$ and $J_x(\mathbf{n};Y) = J_y(\mathbf{n};Y)$ are chosen as in Eq. 3. In these cases, the model becomes a 3-dimensional $Z(2) \times Z(2)$ gauge theory with anisotropic

couplings among plaquettes, which may be called the "Random Coupled-Plaquette Gauge Model (RCPGM)".

A Pauli error on a qubit, which is detected by syndrome measurements, results in the wrong-sign coupling $J_{x,y}$ of the coupling associated with this qubit and a syndrome error results in the wrong-sign coupling J_t's. Then, these statistical mechanics models become variants of quenched disordered spin systems which have many local minima due to the frustration of couplings. This makes standard Monte Carlo simulation difficult to converge. To overcome this problem, we perform parallel tempering steps between Metropolis updates at a given temperature which involves swapping configurations from neighboring temperatures using the Boltzmann weight [13]. Schematically, the Monte Carlo simulation proceeds as: (1) Wrong-sign bond or wrong-sign plaquette interaction configurations for a given Hamiltonian are drawn with a given quenching probability. (2) For the given configuration of interaction couplings, a fixed number of Metropolis steps for the thermalization at each temperature is taken. (3) For the measurement of observables, a certain number of runs for Metropolis updates is taken. In-between these updates, a parallel tempering step [13] between neighboring temperatures starting from high temperature is done. Measurements of the observables are binned in a regular interval between these combined Monte Carlo updates. The whole process is repeated over different quenched interaction configurations. Therefore, two different averages are involved (one over the thermal ensemble and the other over random configurations of wrong-signs) and there may be two different phase transitions: one for thermal transition and the other spin glass transition.

As these spin models are $Z(2)$ gauge theories, the order parameter for the phase diagram study should be a gauge invariant observable due to Elitzur's theorem [14]. Previous studies based on simpler quantum error models ([15], [16]) use the Wilson loop, $\langle W_C \rangle = \langle \prod_{i \in C} \sigma_i \rangle$, where C denotes any closed curve on the lattice and two different behaviors of the Wilson loop as a function of the loop size is used to distinguish the phases. Wang et al. [15] considered whether the Wilson loop follows an area law or a perimeter law to distinguish the phase and studied the transition at $T = 0$ in detail using the homology of error chains. Ohno et al. [17] as well as Kubica et al. [18] investigated the specific heat, in addition to the Wilson loop behavior. Andrist et al. [16] studied the cumulant of the elementary (i.e. smallest area) Wilson loop to locate the thermal transition temperature. In contrast, we use the Polyakov line, $P(i,j) = \prod_t \sigma_t(i,j)$, as the order parameter, which is routinely used in studies of Yang-Mills theory (e.g., [19]) and is closely related to the Wilson loop. Since a first order thermal transition is expected [16], we consider the third order cumulant together with the susceptibility of the Polyakov line,

$$\langle |\overline{P}| \rangle, \quad \overline{P} = \frac{1}{L^2} \sum_{i,j} P(i,j) = \frac{1}{L^2} \sum_{i,j} \prod_t \sigma_t(i,j), \qquad \chi = \langle \tilde{P}^2 \rangle, \qquad B_3 = \langle \tilde{P}^3 \rangle / \langle \tilde{P}^2 \rangle^{3/2}, \tag{8}$$

where (i,j) denotes the space-like sites and $\prod_t$ means taking a product along the time-direction at a given (i,j) and $\tilde{P} = |\overline{P}| - \langle |\overline{P}| \rangle$. Due to periodic boundary conditions, the Polyakov line is gauge-invariant. Since the Polyakov line in our model is a product of Ising spin variables, the Polyakov line at $\mathbf{x}$ itself has $\pm$-sign and $\langle \overline{P} \rangle$ serves as the "average magnetization" over the lattice volume and is less susceptible to short distance fluctuation since the product in Eq. 8 is over the entire time direction.

Fig. 2 shows typical behaviors of the average Polyakov line across different noise probabilities. Without wrong-sign plaquettes (i.e., $p = 2.88 \times 10^{-5}$), the behavior of the average Polyakov line shows a well-defined transition temperature in the infinite volume limit. Well-above the threshold probability (see figures with $p = 0.00852$ in Fig. 2, 3, and 4), the average Polyakov line does not show a transition as the lattice volume increases. Below and near the threshold probability ($p = 0.00682$), the order parameter still shows a transition. The third order cumulant and the susceptibility corroborate this observation. In Fig. 4 and Fig. 3, B_3 crosses zero at the temperature where χ reaches a peak. Well above the threshold probability ($p = 0.00852$), even at low temperature, B_3 does not cross zero and χ does not reach a peak. Between these two extreme noise cases, B_3 crosses zero and χ still shows a peak at a similar temperature. We note that finite volume effects are important near the threshold probability [20]. MC result at $p = 0.020$ (which is not included in Fig. 5) shows a thermal transition but the transition temperature, T_c from $8^3, 12^3, 16^3, 20^3$ and 24^3 keep decreasing as the lattice volume increases and it appears that the infinite volume limit of T_c does not exist.

3. Result

In this section, an investigation of the 2-dimensional toric/sufrace code for quantum memory with realistic circuit-level quantum noise (i.e., bit-flip error and/or phase-flip error on qubits together with syndrome measurement error) is illustrated as an example. The statistical mechanics model which corresponds to this case is 3-dimensional $Z(2)\times Z(2)$ gauge theory with anisotropic couplings and some of the couplings given in Eq. 5 have wrong-signs.

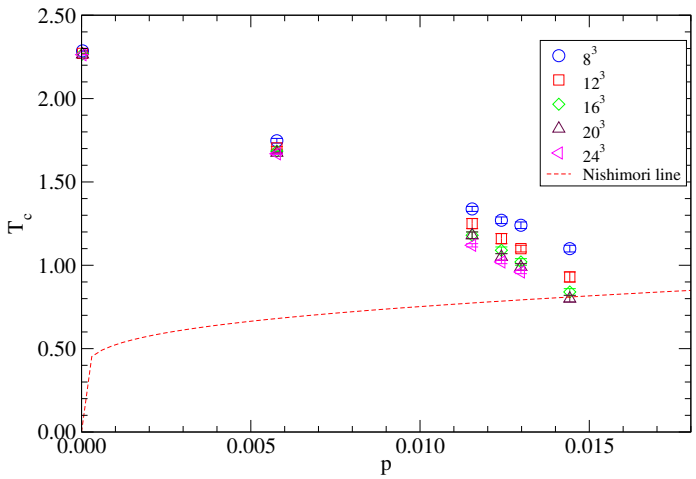

Figure 5: Thermal transition temperature vs. wrong-sign probability on various 3-dimensional lattices for $Z(2)\times Z(2)$ gauge theory which corresponds to the case of a realistic circuit-noise for bit-flip error/phase-flip errors together with syndrome measurement errors.

Fig. 2 shows the behavior of the Polyakov line for the case of $p = 2.88 \times 10^{-5}$ (left) which is well below p_c and for $p = 2.31 \times 10^{-2}$ (right) which is well above p_c (Note that we find that the threshold probability, $p_c \simeq 0.0144$ in this model from the behavior of various observables). Well below the threshold probability, the system shows a sudden jump in the Polyakov line which is in

accordance with a first order transition. With a large quantum error ($p >> p_c$), clearly there is no transition. The behavior of Polyakov line susceptibility, Fig. 3 and the behavior of the third order cumulant of Polyakov line, Fig. 4 agrees with the observation based on the Polyakov line results. The transition temperature can be located by comparing the peak of the susceptibility and the third order cumulant. The thermal transition temperature is tracked as the the wrong-sign probability is increased from smaller p to larger p. T_c vs. p is plotted in Fig. 5.

4. Conclusion

Through Monte Carlo simulation (metropolis steps with parallel tempering steps), we investigate phase diagrams of various versions of $Z(2)$ lattice gauge theories (one of which is Random Coupled-Plaquette Gauge Model (RCPGM) having $Z(2)\times Z(2)$ gauge symmetry) in connection with studying the threshold probability for Quantum Error Correction (QEC) protocol of toric/surface code with data qubit error and syndrome measurement error. The susceptibility and the third order cumulant of the Polyakov line allows us to map the phase transitions in the (T, p) space (temperature and the disorder probability) and locate the threshold probability.

The fault-tolerant implementation of toric/surface code is being hotly pursued (see e.g., the recent work by Google Quantum and AI collaboration [3]). The threshold probability is associated with the decoding problem of QEC. The lattice models studied in this work are results of mapping QEC protocols of toric/surface with the cases of uniform depolarizing noise with syndrome errors, circuit-level noise (specifically independent XZ noise plus syndrome noise) and anisotropic asymmetric depolarizing noise plus syndrome noise into corresponding statistical mechanics models.

The case for QEC of toric/surface code with bit-flip noise (X error) plus syndrome measurement error or with phase-flip noise (Z error) plus syndrome noise is mapped into 3-dimensional anisotropic $Z(2)$ gauge theory. Preliminary result of Monte Carlo simulation shows the threshold probability for this case is $p_c \simeq 0.00682$. The uniform depolarizing noise ($\mathrm{pr}(X) = \mathrm{pr}(Y) = \mathrm{pr}(Z) = 1/3p$) (where Y-erorr is marginalized) plus syndrome noise ($\mathrm{pr}(q) = p$) case in the toric/surface code is mapped into three-dimensional isotropic $Z(2) \times Z(2)$ gauge theory. Again, preliminary Monte Carlo simulation result suggests the threshold probability of $p_c \simeq 0.06$. The most complex case, (X, Y, Z) data error (where $Y-$ error is marginalized) plus syndrome measurement error is mapped into a three-dimensional anisotropic $Z(2) \times Z(2)$ gauge theory. Preliminary Monte Carlo simulation suggests $p_c \simeq 0.0144$. Mapping QEC decoding problems under realistic noise models into statistical mechanics models and studying the threshold probability via Monte Carlo simulation is useful tool for realizing fault-tolerant quantum computer. Extending this method to other QEC codes such as color codes will be explored in the future.

Acknowledgments

SK is supported by the National Research Foundation of Korea under grant NRF-2021-1092701 and in part by NRF-2008-000458 funded by the Korean government and by the IITP(Institute of Information & Coummunications Technology Planning & Evaluation)-ITRC(Information Technology Research Center) grant funded by the Korea government(Ministry of Science and ICT)(IITP-2024-RS-2024-00437191).

References

[1] P.W. Shor, *Algorithms for quantum computation: Discrete logarithms and factoring*, in proceedings of *35th Annual Symposium on Foundations of Computer Science* (1994) 124.

[2] L. Funcke, T. Hartung, K. Jansen and S. Kühn, *Review on Quantum Computing for Lattice Field Theory*, *PoS* **LATTICE2022** (2023) 228 [2302.00467].

[3] Google Quantum AI and Collaborators, *Quantum error correction below the surface code threshold*, 2408.13687.

[4] D.P. DiVincenzo, *The physical implementation of quantum computation*, *Fortsch. Phys.* **48** (2000) 771 [quant-ph/0002077].

[5] Intel, *Delivering resilient and reliable workstations: the role of ECC memory*, workstation-ecc-memory-brief.pdf.

[6] J. Preskill, *Reliable quantum computers*, *Proc. Roy. Soc. Lond. A* **454** (1998) 385 [quant-ph/9705031].

[7] E.T. Campbell, B. M. Terhal, and C. Vuillot, *Roads towards fault-tolerant universal quantum computation*, *Nature* **549** (2017) 172.

[8] R.W. Hamming, *Error detecting and error correcting codes*, *The Bell system technical journal* **29** (1950) 147.

[9] E. Dennis, A. Kitaev, A. Landahl and J. Preskill, *Topological quantum memory*, *J. Math. Phys.* **43** (2002) 4452 [quant-ph/0110143].

[10] D. Vodola, M. Rispler, S. Kim and M. Müller, *Fundamental thresholds of realistic quantum error correction circuits from classical spin models*, *Quantum* **6** (2022) 618 [2104.04847].

[11] M. Rispler, D. Vodola, M. Müller and S. Kim, *The random coupled-plaquette gauge model and the surface code under circuit-level noise*, 2412.14004.

[12] H. Nishimori, *Exact results on spin glass models*, *Physica A* **306** (2002) 68 [cond-mat/0201056].

[13] D.J. Earl and M.W. Deem, *Parallel tempering: Theory, applications, and new perspectives*, *Phys. Chem. Chem. Phys.* **7** (2005) 3910 [physics/0508111].

[14] S. Elitzur, *Impossibility of spontaneously breaking local symmetries*, *Phys. Rev. D* **12** (1975) 3978.

[15] C. Wang, J. Harrington, and J. Preskill, *Confinement-Higgs transition in a disordered gauge theory and the accuracy threshold for quantum memory*, *Annals Phys.* **303** (2003) 31 [quant-ph/0207088].

[16] R.S. Andrist, *Understanding Topological Quantum Error-Correction Codes Using Classical Spin Models*, Doctoral dissertation (2012), ETH Zurich.

[17] Takuya Ohno, Gaku Arakawa, Ikuo Ichinose, and Tet- suo Matsui, *Phase structure of the random-plaquette Z2 gauge model: accuracy threshold for a toric quantum memory*, *Nucl. Phys. B* **697** (2004) 462 [quant-ph/0401101].

[18] A. Kubica, M.E. Beverland, F. Brandão, J. Preskill, and K.M. Svore, *T*hree- Dimensional Color Code Thresholds via Statistical Mechanical Mapping, *Phys. Rev. Lett.* **120** (2018) 180501 [1708.07131].

[19] S. Borsányi, R. Kara, Z. Fodor, D.A. Godzieba, P. Parotto, and D. Sexty, *Precision study of the continuum SU(3) Yang-Mills theory: How to use parallel tempering to improve on supercritical slowing down for first order phase transitions*, *Phys. Rev. D* **105** (2022) 074513 [2202.05234].

[20] K. Binder and D.P. Landau, *Finite-size scaling at first- order phase transitions*, *Phys. Rev. B* **30** (1984) 1477.